



Original scientific paper

Electrochemical corrosion performance of Si-doped Al-based automotive alloy in 0.1 M NaCl solution

Maglub Al Nur¹, Akib Abdullah Khan¹, Somlata Dev Sharma¹ and
Mohammad Salim Kaiser²,✉

¹Department of Mechanical Engineering, Bangladesh University of Engineering and Technology, Dhaka-1000, Bangladesh

²Directorate of Advisory, Extension and Research Services, Bangladesh University of Engineering and Technology, Dhaka-1000, Bangladesh

Corresponding author: ✉ mskaiser@iat.buet.ac.bd; Tel.: +88-02-9663129; Fax: +88-02-9665622

Received: May 6, 2022; Accepted: June 6, 2022; Published: June 13, 2022

Abstract

The aim of this study is to investigate the electrochemical corrosion behavior of Al-Si automotive alloys with different levels of Si doping in 0.1 M NaCl solution at room temperature. The study was performed by electrochemical method, using potentiodynamic polarization and electrochemical impedance spectroscopy techniques. The condition of surfaces was characterized by both optical and scanning electron microscopy. Both the EIS and Tafel analyses revealed that the corrosion resistance was improved with the addition of Si up to the eutectic point, what is due to the formation of protective oxide films. The higher Si added alloys showed lower values of current density, while the corrosion potential was shifted to a more positive direction. For higher Si added alloys, a higher amount of Mg₂Si was formed as precipitates, which tend to form oxides such as SiO₂ and MgO, further protecting the surfaces from corrosion. It can be observed from the micrographs that the scratches from polishing are removed after corrosion. Additionally, the SEM images reveal that corroded surfaces appear to have pits that are less noticeable in alloys with a greater Si content, suggesting thus the formation of a protective layer of oxides.

Keywords

Al-Si automotive alloy; protective oxide layer; corrosion potential; polarization resistance; microstructure

Introduction

Automotive industry focus on lightweight materials like aluminium-silicon alloys for manufacturing automotive components like engine blocks, cylinder heads, pistons, intake manifolds and other parts, replacing steel and cast iron [1-3]. These lightweight materials not only increase fuel efficiency but also enhance properties such as high elongation values, high strength-to-weight ratio, and excellent corrosion resistance [4,5]. Recently, diesel and direct fuel gasoline engines were developed, which have a high specific power. Because of working in diverse environments, these

engines have a significant performance influence on piston materials [6]. Corrosion is the process through which materials, especially metals, gradually deteriorate due to chemical or electrochemical reactions with their surroundings. Corrosion of engine components results in loss of strength, hardness, toughness, and other desirable mechanical properties, which deteriorates engine performance.

Pure Al is highly resistive to corrosion due to a passive film formed on its surface when exposed to the atmosphere. However, in the case of Al alloys, corrosion resistance decreases as various alloying elements are added, such as Cu, Mg and Fe. These alloying elements have their effects on the corrosion properties of Al-Si alloys. One important parameter affecting mechanical properties and corrosion resistance is the silicon content [7,8]. When silicon is added as the major alloying element, the alloy goes into the 4xxx series. The alloy can be hyper-eutectic, eutectic, or hypo-eutectic, depending on the percentage of silicon in it. If there is 12.6 wt.% Si in the Al-Si alloy, it is the eutectic alloy. The alloy is hypo and hyper eutectic if the percentage of Si in the Al-Si alloy is lower and higher than 12.6 wt.%, respectively [9,10]. The mechanical properties of Al-Si alloys are enhanced in higher Si added alloys, but after the eutectic composition, the strength properties start to deteriorate, as coarse polyhedral particles appear after eutectic composition, which is in fact, primary silicon [11]. If Cu is present in the experimental alloys, it helps resist corrosion by forming a protective oxide layer, approximately 900 to 1000 nm thick [12]. The addition of Si along with Mg into the alloy creates the precipitates of Mg_2Si , which facilitate the formation of oxides like SiO_2 and MgO as protective layers. These oxides further protect the surfaces from corrosion [13]. Iron as an alloying element tends to form a iron-rich layer in Fe_2O_3 , which diminishes corrosion resistance [14]. The automotive alloy can get in contact with many solutions. The piston and cylinder of the engine continuously are in contact with engine fuels. Often, some unexpected chemicals may mix with the fuel. Sodium chloride can enter the fuels as sodium careers [15,16]. Also, sodium chloride is present in engine cooling water, which has a deleterious effect on engine materials [17]. One of the key factors of nucleation of pitting is the adsorption of aggressive ions such as Cl^- into the faults in the protective layer and their penetration and accumulation in these imperfections [18,19].

There are some studies about the role of Si as an alloying element on the corrosion resistance, and the effect of NaCl as a corrosive medium for Al-Si alloys. Role of other alloying elements in automotive Al-Si alloys, such as Cu, Mg, Fe, Ni, *etc.*, and investigations of their influence on mechanical and corrosion properties are ongoing. However, there is limited work on the effect of Si on the corrosion behavior of automotive alloys, keeping the percentages of other alloying elements constant. The purpose of the present study is to investigate the corrosion behavior of automotive alloys with various levels of Si, including an alloy with Si as trace impurity, keeping the concentrations of other constituent elements constant, in NaCl solution of 0.1 M strength. The electrochemical investigations have been carried out using the electrochemical impedance spectroscopy (EIS) method, which provides values of solution resistance, polarization resistance, and double-layer capacitance. Besides, the potentiodynamic polarization technique is also used, which provides the values of corrosion current, corrosion potential and corrosion rate.

Experimental

To study the corrosion behavior of Al-based automotive alloy, Si of the different amounts was added to the alloy. For this purpose, commercially pure aluminium (Al 99.750), copper (Cu 99.997), magnesium (Mg 99.80) and Al-50 wt.% Si master alloy ingots were used. The levels of Cu and Mg were kept constant to investigate the effect of Si as an alloying element. Fe, Ni, Sn, Sb, *etc.* were

also present in the alloys as trace impurities. The Shimadzu PDA 7000 optical emission spectrometer was used to determine the chemical composition of the test alloys. The main constituents of five alloys are given in Table 1.

Table 1. Chemical composition of experimental alloys (wt.%)

Alloy	Content, wt.%					
	Si	Cu	Mg	Fe	Ni	Al
Alloy 1	0.244	2.158	0.767	0.211	0.199	Bal
Alloy 2	3.539	2.309	0.784	0.273	0.217	Bal
Alloy 3	6.149	2.113	0.754	0.301	0.264	Bal
Alloy 4	12.656	2.130	0.770	0.311	0.277	Bal
Alloy 5	17.851	2.190	0.755	0.321	0.281	Bal

A natural gas-fired pit furnace and a graphite crucible were used to melt these alloys. To avoid oxidation during melting, a suitable flux cover was used. For the casting, a mild steel mold of $20 \times 200 \times 300$ millimeters was preheated to $250\text{ }^{\circ}\text{C}$. A muffle furnace was used for homogenization, kept at $450\text{ }^{\circ}\text{C}$ for 12 hours, and then air-cooled to relieve stress. The homogenized samples were solutionized at $535\text{ }^{\circ}\text{C}$ for 2 hours. Then the alloys were quenched in salt water to get a super saturated single-phase region. Afterwards, the alloys were machined to remove the natural oxide layer. Rectangular samples of the alloys ($5 \times 5 \times 12$ mm) were machined from the cast products. To achieve a smooth and refined surface, samples were polished using 320, 600, 800, 1200 and 2000 grit emery sheets. All the samples were subjected to age hardening at $200\text{ }^{\circ}\text{C}$ for 4 hours to get the maximum strength [20,21]. A typical digital microscope was used for microstructural observations. The whole experiment was carried out at room temperature, at $25 \pm 1\text{ }^{\circ}\text{C}$. The densities as well as equivalent weights of the alloys were calculated from the chemical composition.

The electrochemical impedance spectroscopy of the experimental alloys was performed using a computerized CH Instrument – Electrochemical Workstation. Analytical reagent grade NaCl was dissolved in deionized water to prepare 0.1 M solution of NaCl. The tests were carried out in a standard three-electrode glass cell with a capacity of 100 mL. Ag/AgCl-KCl was used as a reference electrode, a platinum electrode was employed as a counter electrode and an experimental alloy sample was used as a working electrode. Only 4×4 millimeters of the surface of each working electrode was exposed to NaCl solution, while the remaining surface was coated with PVC heat shrink tube. A thin wire was connected to the working electrode to complete the circuit. The working electrode was immersed in 100 mL of NaCl solution, and about 30 min of time interval was given to the system to attain a steady-state. The OCP values of samples were determined by measuring the voltage between the working and reference electrodes by the electrochemical workstation. Before EIS analysis, the sinusoidal voltage amplitude was set to 5 mV, and the frequency range from 100 kHz to 0.2 Hz was explored. NaCl solution was refilled periodically during the experimental runs to ensure more precision. The EIS experiments were performed at open circuit potential values, and impedance data were collected for the above-mentioned frequency range. Afterwards, analogous electrical circuits were designed using the data analysis program EC-Lab Analyst. Equivalent circuits were matched to experimental data, and the circuit with maximum accuracy was selected. Thus, the values of the respective circuit components, *i.e.*, solution resistance (R_s), corrosion resistance (R_p), and effective double-layer capacitance ($C_{P(\text{eff})}$), were calculated. Moreover, the goodness of fits was determined from discrepancies between the experimental and fitted data.

Using the same experimental setup as for the EIS, the potentiodynamic polarization experiments were performed similarly. The potential range against the reference electrode was adjusted at -1 to +1 V. The scan rate was set at 0.50 mV s⁻¹. Following the conclusion of the experiment, the relevant Tafel polarization plots were plotted. For each of the experimental alloys, the corrosion potential (E_{corr}) in mV, the corrosion current (I_{corr}) in μ A, and the corrosion rate in millimeters per year were determined using the Tafel polarization plot. After the experiment, the sample surfaces were degraded and examined using a conventional optical microscope and a scanning electron microscope. The formula for determining the corrosion rate in mm year⁻¹ is in accordance with ASTM Standard G 102 defined as:

$$\text{Corrosion rate} = \frac{I_{corr} K EW}{\rho A} \quad (1)$$

where I_{corr} = corrosion current in A, K = constant defining the units of corrosion rate in mm year⁻¹ (here, $K = 3272 \text{ mm (A cm year)}^{-1}$ from ASTM Standard G 102), EW = equivalent weight in gram/equivalent, ρ = density of alloy in g cm⁻³ and A = surface area in cm².

Results and discussion

Impedance measurements

Results calculated by fitting the equivalent circuit to experimental data are listed in Table 2. A few circuits were modeled to fit experimental EIS data, and the best-fitted one is presented in Figure 1. R_p denotes the polarization or corrosion resistance equivalent to charge transfer resistance, R_s denotes the ohmic solution resistance of the electrolyte and $C_{p(eff)}$ represents effective electrical double layer capacitance, which impedance is sometimes replaced by the impedance of the constant phase element. It can be noted that the values of R_s are negligible compared to those of R_p . Polarization resistance is related to the working electrode, while solution resistance, here of 0.1 M NaCl, is related mostly to the uncompensated resistance of the electrolyte solution between working and reference electrodes. Results of previous studies indicated that polarization resistance is inversely related to the corrosion rate of a metal, which gives information about the rate of reactivity of the surface with the environment [22-25]. From the data given in Table 2, it can be seen that the value of polarization resistance increases for higher silicon-added alloys up to the eutectic composition of 12.7Si. In other words, the corrosion rate decreases up to the eutectic point, making 12.7Si the most corrosion resistant alloy among the samples. According to previous studies, the OCP value increases or shifts toward a more positive value as corrosion resistance increases. Hence, a more positive value of OCP means higher corrosion resistance [22]. From the experimental data, the values of the open circuit potential shift to a more positive direction for higher Si-added alloys. The effective double-layer capacitance ($C_{p(eff)}$) value decreases to 12.7Si, then it increases to 17.9Si.

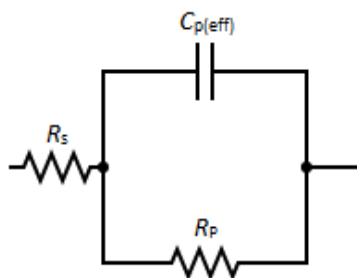
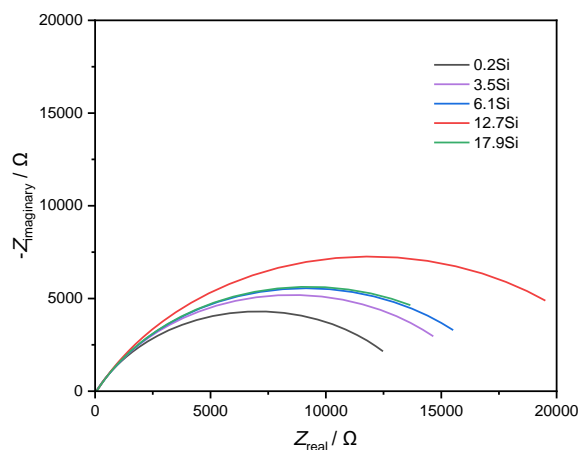


Figure 1. Equivalent electrical circuit used to fit EIS data of automotive Al-Si alloys

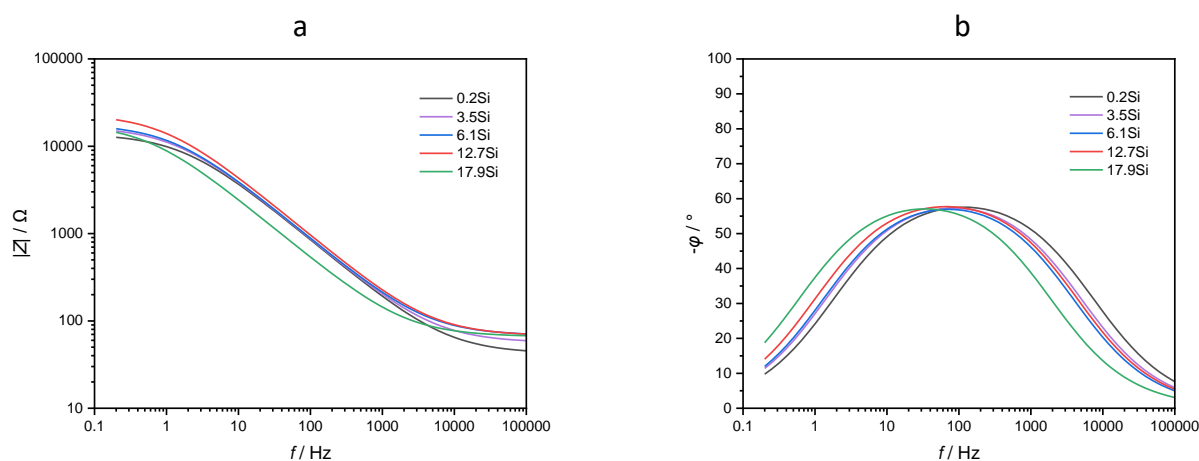
Table 2. Test results from electrochemical impedance spectroscopy (EIS) and OCP values

Alloy	OCP, V vs. SCE	R_s / Ω	R_p / Ω	$C_{p(\text{eff})} / \mu\text{F}$	Goodness of fit
Alloy 1 (0.2Si)	-0.66048	42	14040	12.91	0.04703
Alloy 2 (3.5Si)	-0.65451	55.97	16947	12.75	0.07666
Alloy 3 (6.1Si)	-0.64811	67.56	18121	12.62	0.06434
Alloy 4 (12.7Si)	-0.63539	66.91	23708	11.62	0.0257
Alloy 5 (17.9Si)	-0.62005	65.72	18379	21.51	0.06588

Figure 2 shows Nyquist diagrams of the experimental impedance measurements for all the automotive Al-Si alloys immersed in 0.1 M NaCl solution. The real (Z_{real}) and imaginary ($-Z_{\text{imaginary}}$) parts of the impedance are represented at the x and y axes, respectively. For each of the experimental alloys, the imaginary component of the impedance ($-Z_{\text{imaginary}}$) against the real part (Z_{real}) is derived using the capacitive-resistive model. A single full semicircular appearance on the Nyquist diagram indicates that the corrosion of Al-Si alloy is regulated by the charge transfer process [26]. Small distortion in diagrams may be due to frequency dispersion [25]. Figure 2 shows Nyquist plots that are slightly depressed, indicating that they are not perfect semicircles as expected by EIS theory. This discrepancy can be explained by the non-ideal behavior of the double layer as a capacitor [27,28].

**Figure 2.** Nyquist plots for experimental automotive alloys in 0.1 M NaCl solution at room temperature

The impedance data obtained are displayed as Bode plots in Figure 3. The Bode magnitude plot displays the impedance modulus versus frequency (Figure 3(a)), and the Bode phase plot displays the phase angle versus frequency (Figure 3(b)).

**Figure 3.** Bode plots for experimental alloys: (a) Bode magnitude plots ($|Z|$ vs. frequency), (b) Bode phase plot (phase angle vs. frequency)

Potentiodynamic polarization analysis

The Tafel plots or potentiodynamic polarization curves of the aluminium-silicon alloys with varying concentrations of silicon are shown in Figure 4. Table 3 displays the parameters obtained from the potentiodynamic polarization analysis. I_{corr} represents the corrosion current, which is the dissolution current at the corrosion potential. The corrosion potential, E_{corr} is a mixed potential in which the rate of anodic dissolution equals the rate of cathodic reactions, and there is no net current flowing in or out of the electrode. This potential is also known as open circuit potential or rest potential [29]. E_{corr} represents the ability of metal and nonmetal surfaces to lose electrons in the presence of an electrolyte, and the corrosion rate is shown in mm/y, which is the amount of corrosion loss in thickness per year. It can be interpreted that both the corrosion current and corrosion rate decrease as the concentration of Si is increased up to 12.7 wt.%, and then increase again for the alloy with 17.9 wt.% Si. According to the chemical composition, there is about 0.8 wt.% Mg in each of the alloys and so, in higher Si added alloys, the amount of Mg_2Si formed is higher. This intermetallic phase is added to a protective layer as oxides, which disrupt the corrosion process [13]. The results from previous investigations prove the presence of Al_2O_3 when electrochemical corrosion occurs at surfaces of Al-Si alloys in 0.1 M NaCl [30]. Again, Si addition may allow the formation of Fe_2SiAl_7 interdiffusion layer, limiting the growth of Fe-Al intermetallic phases [30]. However, such intermetallic layers only provide barrier protection, not cathodic protection [31]. To be added, the thickness of the diffusion layer has been considered an important factor for better corrosion performance, as the Al-Si coating is susceptible to microcrack due to different thermal expansion coefficients between coating and substrate.

Table 3. Corrosion parameters resulted from potentiodynamic polarization analysis

Alloy	$I_{corr} / \mu A$	E_{corr} / mV	Corrosion rate, mm year ⁻¹
Alloy 1 (0.2Si)	20.178	-597.538	0.8858
Alloy 2 (3.5Si)	18.156	-583.639	0.7954
Alloy 3 (6.1Si)	17.321	-583.112	0.7575
Alloy 4 (12.7Si)	13.491	-574.055	0.5865
Alloy 5 (17.9Si)	17.845	-577.849	0.771

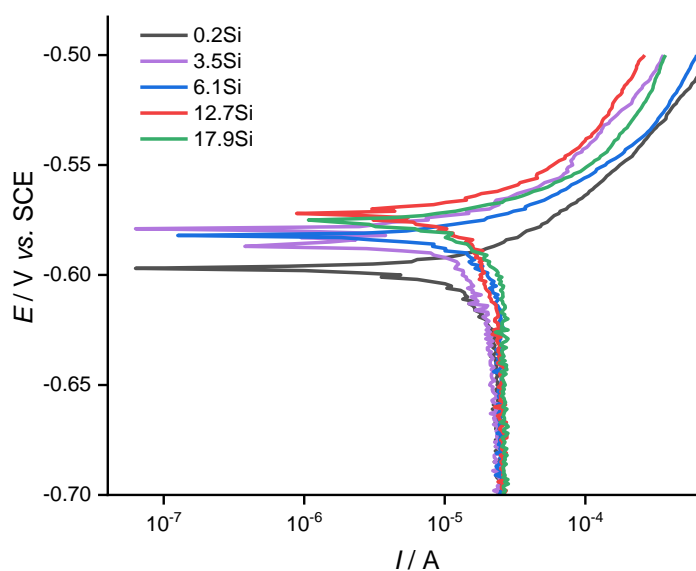


Figure 4. Potentiodynamic polarization curves of automotive Al-Si alloys with varying levels of Si tested in 0.1 M NaCl

The microcracks do not propagate through thick diffusion layers [32,33]. The Mg_2Si phase allows cathodic protection, enhancing the anti-corrosion performance of Al-Si alloys. From the values of corrosion potential (E_{corr}), it is found that the values shift towards a more positive direction for higher Si added alloys, up to a eutectic point, which indicates better corrosion performance in higher Si added alloys [34]. An exception is noted in the case of 17.9Si added alloy. The probable reason is that beyond the eutectic composition, more primary Si is created in the matrix, which has needles or plate-like Al-Si eutectic. These structures are dispersed in such a way that creates pores on the surfaces of the alloys. As a result, excess corrosion occurs at the sites where pores exist. Again, because of Mg_2Si particles, the alloy is more prone to localized corrosion [35]. The minor scatter in the potentiodynamic curves could be due to surface conditions such as surface porosity, the existence of un-melted powder, and the density of melt pool borders at the surface [36].

Optical micrographic investigation

Figure 5 shows optical micrographs of the polished surfaces of 0.2Si, 3.5Si, 6.1Si, 12.7Si and 17.9Si doped experimental alloys before and after corrosion in 0.1 M NaCl solution. Not enough information can be extracted from these types of unetched microstructures, but some apparent observations can be made. There are Al-rich dendritic matrix, eutectic Si, and some different intermetallic phases in these microstructures. In this type of image, precipitations of Fe and Cu with Al appear in a darker tone, whereas Si and Mg with Al appear in a lighter tone. As a result of the varying quantities of Si, the alloys display different levels of tone, which is visible in Figure 5. As the experimental alloys went through the electrochemical corrosion process, corrosion was observed on the surfaces at different intensities according to Si concentration. Optical micrographs of the surfaces of the alloys after corrosion presented in Figure 5 show concentrated attacks on different locations of each experimental alloy surface, generated by corrosion products dissolving into the surrounding environment, *i.e.*, 0.1 M NaCl solution.

Comparing the micrographs of the surfaces of the alloys before and after corrosion, it is visible that the polished marks completely disappeared after corrosion. The corroded surfaces seem to have pit formations that are lower for higher Si-added alloys. The factor controlling this characteristic might be the intermetallics containing Si, one of which is Mg_2Si . This intermetallic tends to form MgO and SiO_2 during corrosion, serving as protective films which are thicker for higher Si-added alloys [13,30]. Besides, Al_2O_3 and $Al(OH)_3$ are also formed as a protective coating in every experimental automotive alloy [30,37,38]. The formation of pits may be attributed to the fact that the intermetallics fall off the surfaces due to the dissolution of the surrounding matrix. It is noted that the surface of the 17.9Si added alloy exhibits the most obliteration among the surfaces of all experimental alloys, which is due to the increased amount of primary silicon in that alloy. Increased surface pinholes can be discerned on the surfaces of the hypereutectic alloy, which may be attributed to intermetallic particles created by high impurity. These surface pinholes indicate an excessive pitting corrosion mechanism [39].

SEM and EDX observations

Figure 6 shows the surface morphology of corroded surfaces of various Si-added experimental alloys after electrochemical corrosion in 0.1 M NaCl solution using SEM images. SEM photographs prove the corrosion of intermetallic compounds on the surface of each of the experimental alloys. In higher Si added alloys, the rough polish marks are more visible, except in the 17.9Si alloy, as corrosion is more prominent in that alloy. Moreover, numerous surface defects as pinholes are also identified in the SEM image of 17.9Si added sample, similar to the optical image.

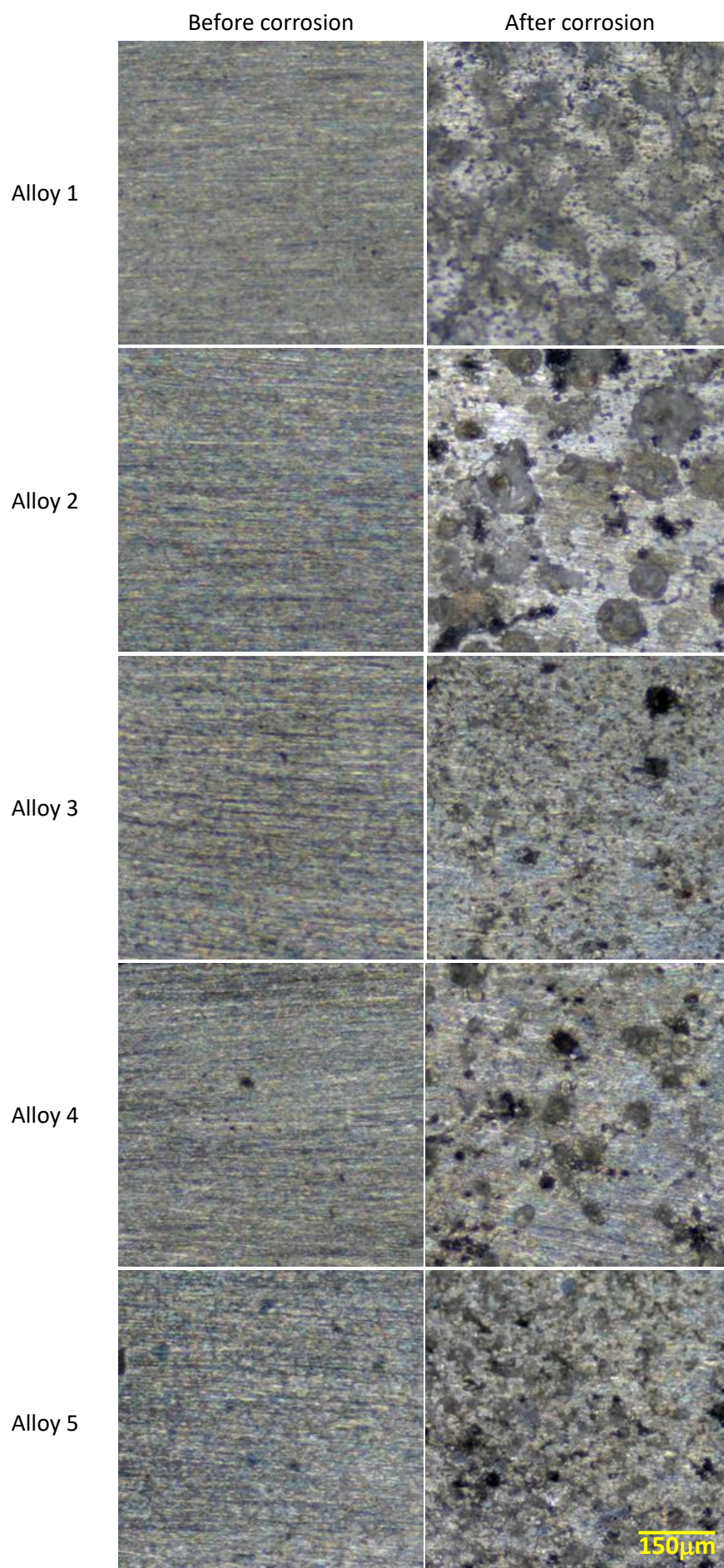


Figure 5. Microstructure of polished Al-Si alloys before and after corrosion in 0.1 M NaCl solution

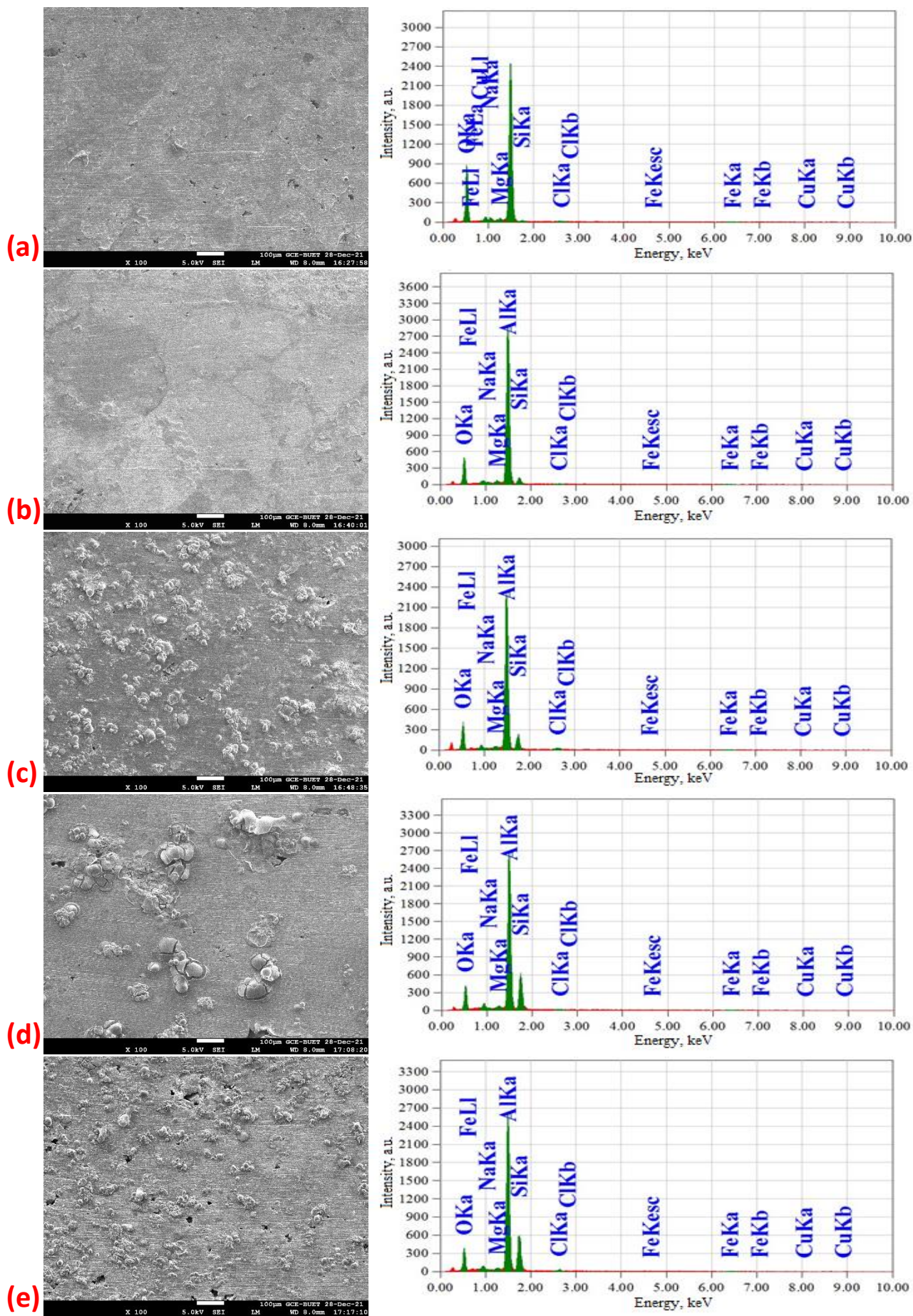


Figure 6. SEM images and EDX spectra of Al-Si alloys after exposure to 0.1 M NaCl solution: (a) 0.2Si, (b) 3.5Si, (c) 6.1Si, (d) 12.7Si, (e) 17.9Si

Selective dissolution of primary aluminium phases over a depth of a few micrometers creates the pinholes [39]. The images prove that there are localized corrosion and discrete pits on the surfaces of the samples. More pits can be identified in the lower Si added alloys, indicating their less resistivity to corrosion. Pit development is most likely the result of intermetallic compounds dissolving from the alloy surface into the surrounding environment. It is also possible that the pits are formed as a result of selective dissipation of the alloy second phase particles. Because there was no dissolution of corrosion products into the surrounding matrix, the majority of corrosion products are visible on the surfaces in SEM photographs. The corrosion products that occur on the surfaces are dispersed unevenly. A protective layer is also observable on the surface of every corroded alloy, which seems to be thicker in higher Si-added alloys. Overall, the SEM images dictate that the corrosive property is improved as Si is added into automotive alloys if other constituent alloying elements are kept fixed up to the eutectic point.

From the quantitative EDX analysis the alloys show following chemical compositions in wt. %:

0.2 Si added Alloy 1: 27.25 % O, 0.46 % Mg, 0.74 % Si

3.5 Si added Alloy 2: 14.75 % O, 0.74 % Mg, 4.64 % Si

6.1 Si added Alloy 3: 13.70 % O, 0.50 % Mg, 9.81 % Si

12.7 Si added Alloy 4: 11.37 % O, 0.55 % Mg, 21.17 % Si

17.9 Si added Alloy 5: 10.73 % O, 0.58 % Mg, 21.53 % Si

One interesting observation is that the percentage of oxygen decreases at higher Si-added alloys. As wt.% of Si is increased, more elements from the surface are depleted as oxides, and the corrosion products remain on the surface, which is the reason for the higher percentage of oxygen in lower silicon-added alloys. EDX data shows the oxygen percentage decreases even after the eutectic point, the trend not aligning with the previous results.

The probable reason is that oxides are formed due to Si, which follows the same trend in the hypereutectic alloy. But the corrosion is not protected the same way after the eutectic point for the surface defects created. Another observation is that the wt.% of Si and Mg is more than the wt.% found from the chemical composition determined by the spectrometer in every alloy. Although other elements are dissolved into the solution, increased Si does not dissolve and forms Mg_2Si , which is involved in protecting the materials from corrosion, as discussed earlier.

Conclusions

Based on the above discussions, the following conclusions are emphasized:

Alloys with higher Si content have better corrosion resistance up to eutectic composition if other components are kept constant. It occurs due to the formation of protective layers of SiO_2 and MgO by Mg_2Si , which is more pronounced in higher Si-added alloys. Beyond eutectic composition, the corrosion resistance tends to fall since the plate-like morphology of hyper-eutectic intermetallic results in surface pinholes.

It is observed that the surfaces are demolished to some extent after corrosion. Again, observing the optical micrographs and SEM images, the surface deterioration seems lesser in higher Si added alloys but exceptionally higher in 17.9Si added alloy. Oxide layers are formed after corrosion for all alloys, but the layers are thicker in higher Si-added alloys, which is visible in both optical and SEM images. The percentage of oxygen on the surface of an alloy is less for higher Si added alloy, as less corrosion product is formed.

Differences in electrochemical behavior appeared due to differences in their chemical compositions and microstructures. The percentage of Si as alloying element determines the overall corrosion behavior of as-cast Al-Si alloys in this study.

Acknowledgements: It is supported by the Department of Mechanical Engineering of Bangladesh University of Engineering and Technology, Dhaka. Thanks to Department of Chemistry for the laboratory facilities.

References

- [1] S. Samat, M. Z. Omar, A. H. Baghdadi, I. F. Mohamed, A. M. Aziz, *Journal of Materials Research and Technology* **10** (2021) 1086-1102. <https://dx.doi.org/10.1016/j.jmrt.2020.12.085>
- [2] H. Ye, *Journal of Materials Engineering and Performance* **12** (2003) 288-297. <https://dx.doi.org/10.1361/105994903770343132>
- [3] M. Guo, M. Sun, J. Huang, S. Pang, *Metals* **12** (2022) 142. <https://dx.doi.org/10.3390/met12010142>
- [4] L. F. Gomes, C. L. Kugelmeier, A. Garcia, C. A. Della Rovere, J. E. Spinelli, *Journal of Materials Research and Technology* **15** (2021) 5880-5893. <https://dx.doi.org/10.1016/j.jmrt.2021.11.043>
- [5] W. Miller, L. Zhuang, J. Bottema, A. Wittebrood, P. De Smet, A. Haszler, A. Viergge, *Materials Science and Engineering: A* **280** (2000) 37-49. [https://dx.doi.org/10.1016/S0921-5093\(99\)00653-X](https://dx.doi.org/10.1016/S0921-5093(99)00653-X)
- [6] T. Tanaka, T. Akasawa, *Journal of Materials Engineering and Performance* **8** (1999) 463-468. <https://dx.doi.org/10.1361/105994999770346774>
- [7] P. R. Goulart, J. E. Spinelli, W. R. Osório, A. Garcia, *Materials Science and Engineering: A* **421** (2006) 245-253. <https://dx.doi.org/10.1016/j.msea.2006.01.050>
- [8] S. Tahamtan, A. Fadavi Boostani, *Transactions of Nonferrous Metals Society of China* **20** (2010) 1702-1706. [https://dx.doi.org/10.1016/S1003-6326\(09\)60361-7](https://dx.doi.org/10.1016/S1003-6326(09)60361-7)
- [9] M. Haghshenas, J. Jamali, *Case Studies in Engineering Failure Analysis* **8** (2017) 11-20. <https://dx.doi.org/10.1016/j.csefa.2016.11.003>
- [10] F. Alshmri, *Advanced Materials Research* **774-776** (2013) 1271-1276. <https://dx.doi.org/10.4028/www.scientific.net/AMR.774-776.1271>
- [11] H. Torabian, J. P. Pathak, S. N. Tiwari, *Wear* **172** (1994) 49-58. [https://dx.doi.org/10.1016/0043-1648\(94\)90298-4](https://dx.doi.org/10.1016/0043-1648(94)90298-4)
- [12] A. Schüssler, H. E. Exner, *Corrosion Science* **34** (1993) 1793-1802. [https://dx.doi.org/10.1016/0010-938X\(93\)90017-B](https://dx.doi.org/10.1016/0010-938X(93)90017-B)
- [13] R. Escalera-Lozano, M. I. Pech-Canul, M. A. Pech-Canul, M. Montoya-Davila, A. Uribe-Salas, *The Open Corrosion Journal* **3** (2010) 73-79. <https://dx.doi.org/10.2174/1876503301003010073>
- [14] L. Wen, Y. Wang, Y. Zhou, L. X. Guo, J. H. Ouyang, *Materials Chemistry and Physics* **126** (2011) 301-309. <https://dx.doi.org/10.1016/j.matchemphys.2010.11.022>
- [15] M. D. Cardenas Almena, O. Lucio Esperilla, F. Martin Manzanero, Y. Murillo Duarte, L. C. Quintero Toscano, G. Wolff, *SAE Technical paper* 2012-01-1689, 2012. <https://dx.doi.org/10.4271/2012-01-1689>
- [16] J. Barker, S. Cook, P. Richards, *SAE International Journal of Fuels and Lubricants* **6** (2013) 826-838. <https://dx.doi.org/10.4271/2013-01-2687>
- [17] A. Abdel-Wahab, B. Batchelor, *Water Environment Research* **74** (2002) 256-263. <https://dx.doi.org/10.2175/106143002X139983>

- [18] P. Marcus, *Corrosion Mechanism in Theory and Practice*, J. Oudar (Ed.), Marcel Dekker, New York, 1995. ISBN-10: 082479592X
- [19] E. S. M. Sherif, *International Journal of Electrochemical Science* **7** (2012) 4235-4249. <http://www.electrochemsci.org/papers/vol7/7054235.pdf>
- [20] S. Toschi, *Metals* **8** (2018) 961. <https://dx.doi.org/10.3390/met8110961>
- [21] M. S. Kaiser, M. R. Basher, A. S. W. Kurny, *Journal of Materials Engineering and Performance* **21** (2012) 1504-1508. <https://dx.doi.org/10.1007/s11665-011-0057-3>
- [22] S. Choudhary, A. Garg, K. Mondal, *Journal of Materials Engineering and Performance* **25** (2016) 2969-2976. <https://dx.doi.org/10.1007/s11665-016-2112-6>
- [23] A. Hossain, M.A. Gafur, F. Gulshan, A.S.W. Kurny, *International Journal of Chemical, Nuclear, Materials and Metallurgical Engineering* **8** (2014) 719-723.
- [24] A. S. Fouda, F. S. Mohamed, M. W. El-Sherbeni, *Journal of Bio- and Tribo-Corrosion* **2** (2016) 11. <https://dx.doi.org/10.1007/s40735-016-0039-y>
- [25] J. Bessone, C. Mayer, K. Jüttner, W. J. Lorenz, *Electrochimica Acta* **28** (1983) 171-175. [https://dx.doi.org/10.1016/0013-4686\(83\)85105-6](https://dx.doi.org/10.1016/0013-4686(83)85105-6)
- [26] X. Li, S. Deng, H. Fu, G. Mu, *Corrosion Science* **51** (2009) 620-634. <https://dx.doi.org/10.1016/j.corsci.2008.12.021>
- [27] J. Cruz, T. Pandiyan, E. García-Ochoa, *Journal of Electroanalytical Chemistry* **583** (2005) 8-16. <https://dx.doi.org/10.1016/j.jelechem.2005.02.026>
- [28] W. A. W. E. Amira, A. A. Rahim, H. Osman, K. Awang, P.B. Raja, *International Journal of Electrochemical Science* **6** (2011) 2998-3016. <https://dx.doi.org/10.1.1.655.3240>
- [29] X. G. Zhang, *Corrosion Potential and Corrosion Current in: Corrosion and Electrochemistry of Zinc*, Springer US, Boston, MA, 1996, pp. 125-156. https://dx.doi.org/10.1007/978-1-4757-9877-7_5.
- [30] C. Kim, S. Cho, W. Yang, A. I. Karayan, H. Castaneda, *Corrosion Science* **183** (2021) 109339. <https://dx.doi.org/10.1016/j.corsci.2021.109339>
- [31] L. Dosdat, J. Petitjean, T. Vietoris, O. Clauzeau, *Steel Research International* **82** (2011) 726-733. <https://dx.doi.org/10.1002/srin.201000291>
- [32] E. Billur, *Hot Stamping of Ultra High-Strength Steels*, Springer International Publishing, Cham, 2019. <https://dx.doi.org/10.1007/978-3-319-98870-2>
- [33] Y.-Y. Chang, C.-C. Tsaur, J.C. Rock, *Surface and Coatings Technology* **200** (2006) 6588-6593. <https://dx.doi.org/10.1016/j.surfcoat.2005.11.038>
- [34] M. Abdallah, E. M. Kamar, S. Eid, A. Y. El-Etre, *Journal of Molecular Liquids* **220** (2016) 755-761. <https://dx.doi.org/10.1016/j.molliq.2016.04.062>
- [35] F. Eckermann, T. Suter, P. J. Uggowitzer, A. Afseth, P. Schmutz, *Electrochimica Acta* **54** (2008) 844-855. <https://dx.doi.org/10.1016/j.electacta.2008.05.078>
- [36] R. I. Revilla, J. Liang, S. Godet, I. De Graeve, *Journal of The Electrochemical Society* **164** (2017) C27-C35. <https://dx.doi.org/10.1149/2.0461702jes>
- [37] I.-W. Huang, B. L. Hurley, F. Yang, R.G. Buchheit, *Electrochimica Acta* **199** (2016) 242-253. <https://dx.doi.org/10.1016/j.electacta.2016.03.125>
- [38] G. Šekularac, I. Milošev, *Corrosion Science* **144** (2018) 54-73. <https://dx.doi.org/10.1016/j.corsci.2018.08.038>
- [39] M. G. Mueller, M. Fornabaio, A. Mortensen, *Journal of Materials Science* **52** (2017) 858-868. <https://dx.doi.org/10.1007/s10853-016-0381-y>